This article has been accepted for inclusion in a future issue of this journal. Content is final as presented, with the exception of pagination.

Scanning Tunneling Microscope Control: A Self-Tuning PI Controller Based on Online Local Barrier Height Estimation*

Farid Tajaddodianfar, S. O. Reza Moheimani, *Fellow, IEEE,* and John N. Randall, *Fellow, IEEE,*

***Abstract*— We identify the dynamics of a scanning tunneling microscope (STM) in closed loop and show that the plant dc gain is proportional to the square root of local barrier height (LBH), a quantum mechanical property of the sample and/or tip that affects the tunneling current. We demonstrate that during a scan, the LBH may undergo significant variations and this can adversely affect the closed-loop stability if the controller parameters remain fixed. Feedback instabilities increase the risk of tip-sample crash in STMs. In order to improve the closed-loop performance, we estimate the LBH, on the fly, and use that to adaptively tune the proportional-integral (PI) controller parameters. Experimental results obtained with the self-tuning PI controller confirm the improved STM performance compared to the conventional fixed-gain PI controller. Additional experiments confirm effectiveness of the proposed method in extending the tip lifetime by lowering the chance of a tip/sample crash.**

***Index Terms*— Lyapunov filter, local barrier height (LBH), parameter estimation, proportional-integral (PI) controller, scanning tunneling microscope (STM), self-tuning, work function.**

I. Introduction

IN SCANNING probe microscopy, an extremely sharp probing tip is moved over a sample to collect surface topography information taking advantage of a physical phenomenon that takes place between the tip and sample. In scanning tunneling microscope (STM), this phenomenon is the tunneling current, a quantum mechanical effect that refers to the electrical current established due to the tunneling of electrons through the space between a conducting tip and surface when their relative distance is below a nanometer and a bias dc voltage is established between them. This current is modeled as an exponential function of the tip-sample distance. While scanning, atomic-scale surface features cause a change in the tunneling current.

Manuscript received March 16, 2018; accepted May 23, 2018. Manuscript received in final form June 3, 2018. This work was supported by Air Force Research Laboratory and the Defense Advanced Research Project Agency under AFRL Contract #FA8650-15-C-7542. Recommended by Associate Editor I. Petersen. *(Corresponding author: S. O. Reza Moheimani.)*

F. Tajaddodianfar is with Microsoft, Redmond, WA 98052 USA (e-mail: farid.tajaddodianfar@microsoft.com).

S. O. R. Moheimani is with the Department of Mechanical Engineering, Erik Jonsson School of Engineering and Computer Science, University of Texas at Dallas, Richardson, TX 75080 USA (e-mail:reza.moheimani@utdallas.edu).

J. N. Randall is with the Zyvex Labs LLC, Richardson, TX 75081 USA (e-mail: jrandall@zyvexlabs.com).

Color versions of one or more of the figures in this paper are available online at http://ieeexplore.ieee.org.

Digital Object Identifier 10.1109/TCST.2018.2844781

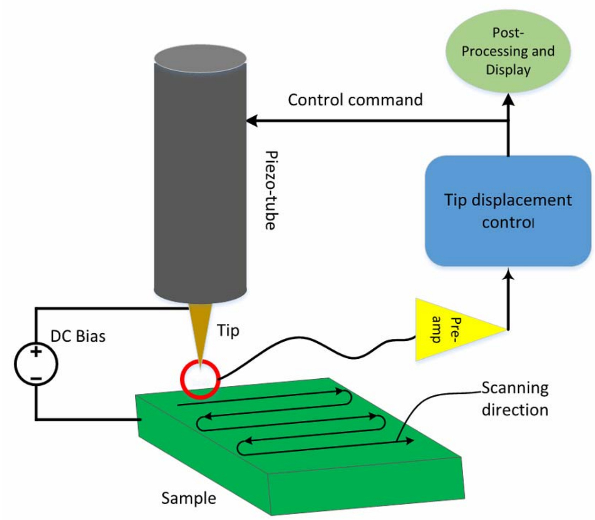

Fig. 1. Schematic of STM operating in constant current mode.

A control system measures this current and adjusts the vertical tip position to compensate for the current variations and keep the current constant. Thus, the controller command maps a topography of the surface. Fig. 1 displays a schematic of the STM operation in the constant current mode.

Over the past three decades, the STM has found a myriad of applications in numerous fields leading to ground-breaking observations (see [1]–[4]). The early works on STM concentrated on imaging. However, soon it was realized that the STM tip could be used as an effective tool for patterning the surface with a resolution down to a single atom through lithography [5]. Atomic-scale lithography continues to be an active research topic in nanotechnology [6]–[9].

Poor performance of the STM control system results in tip-sample crash, a prevalent failure in STMs. Few attempts have been made to improve the STM control system. Oliva *et al*. [10] analyzed the STM control system to obtain optimal imaging conditions [11] and determine optimal feedback parameters [12]. Ahmad *et al.* [13], [14] discussed the design of a robust controller for STM. Bonnail *et al.* [15] modeled the STM control system and proposed a sliding mode scheme for switching between positive and negative feedback control in order to improve the stability.

Blanvillain *et al.* [16] used the tunneling junction to build a sub-nanometer-resolution position sensor which takes advantage of a control system similar to that of the STM. Recently, we showed that the stability of the STM control system is affected by variations in the local barrier height (LBH), a quantum mechanical property of the tip and sample [17]–[20]. The LBH variation has long been known to the STM researchers [21]–[26]. However, to the authors' best knowledge, its adverse effects on the robustness of the STM control system have never been reported.

In this paper, we present further analysis and experiments to support the observation that LBH variations lead to changes in the feedback control loop gain, with adverse effects on the STM closed-loop stability. We use the joint input-output approach [27] to determine frequency response of the closed-loop system. We demonstrate that LBH variations affect the dc gain of the identified open-loop transfer function (TF). Furthermore, we investigate stability of the STM closed-loop system under proportional-integral (PI) control and show that LBH variations may lead to instabilities if PI gains are fixed. Based on this analysis, we propose a self-tuning PI controller that continuously adjusts PI gains according to the LBH measurements in order to prevent instability. We present experimental results showing that the LBH is a varying parameter that depends on both tip and sample properties. Moreover, we present experimental results confirming the enhanced stability and extended tip lifetime under the proposed control method.

In the remainder of this paper, we briefly discuss the theory of tunneling current and present the control system architecture in Section II. Then in Section III, we discuss a method for closed-loop system identification. In Section IV, we discuss online estimation of the LBH and describe the self-tuning PI controller. Section V continues with experimental results. Final conclusions and remarks are given in Section VI.

II. Control System Structure of STM

In this section, we briefly describe the custom-designed STM that was used in our experiments. We also briefly discuss the tunneling current physics and the control system architecture of the existing STM.

A. Experimental Setup

The STM control system runs on a 20-bit digital signal processor operating at 50-kHz sampling frequency. This system is used for all data acquisition and control purposes and is commercially known as ZyVector. A Femto DLPCA-200 transimpedance preamplifier is used to detect the tunneling current. For frequency-domain measurements, we used an ONOSOKKI CF-9400 FFT analyzer. In addition, some of the time-domain measurements were collected by a dSpace Microlab Box. Further details of the experimental setup are described in [17].

B. Tunneling Current and the LBH

Quantum mechanical calculations suggest that the electrical current which tunnels through the vacuum between an STM tip and sample is proportional to the applied bias voltage and is an exponential function of the tip-sample separation [22], [28]. A simplified model is [24]

$$i = \sigma V_b e^{-1.025\sqrt{\varphi}\delta} \tag{1}$$

where V_b is the bias voltage, σ is a parameter depending on the material and geometry of the tip and sample, and δ (in $\mathring{A}$) is the energy barrier thickness which is approximately equal to the geometrical tip-sample separation [24]. φ (in eV) is called "work function" or "Barrier height" which by definition is the minimum energy required to remove an electron from a solid. In quantum mechanics, energy of electron in vacuum is higher than its energy in solid and this difference, i.e., the work function, acts as a barrier preventing electrons from leaving the solid [22], [29]. A preamplifier of gain R is used to convert the sub-nanoampere range tunneling current i in (1) to a measurable voltage, the natural logarithm of which is then taken to linearize the model. This gives

$$\ln(\mathrm{Ri}) = \ln(\mathrm{R}\sigma \mathrm{V_b}) - 1.025\sqrt{\varphi}\delta \tag{2}$$

which indicates that for constant σ and V_b the logarithm of tunneling current is proportional to the tip-sample separation, assuming that φ is constant. This linear relationship between $\ln i$ and δ is crucial to the operation of STM which ultimately maps a surface topography correlated with δ by keeping the current constant using a linear feedback.

In addition, (2) suggests that, for constant σ and V_b, the logarithmic derivative of current with respect to the tip-sample separation provides a measure of the barrier height [21], [24], [30]

$$\varphi = 0.952\left(\frac{d}{d\delta}\ln \mathrm{Ri}\right)^2. \tag{3}$$

It is well understood that the barrier height depends on the physical properties of the tip apex as well as those of the sample surface atoms into which the current tunnels [24]. Thus, the barrier height is a local effect and is subject to change. Based on this understanding, parameter φ can be used to produce another image. This is referred to as the LBH image, and provides additional information about the physical and chemical surface characteristics [22], [23], [31], [32].

Experimental investigations have shown that, for the range of tip-sample separation δ over which the STM usually operates, φ is nearly independent of δ [21], [23], [24]. This assures that the linearization provided by (2) remains effective for normal operating conditions in STM.

C. Closed-Loop Structure

The effective instantaneous tip-sample gap, δ, can be described as

$$\delta = d_{\mathrm{hm}} - d_0 - h - d_{\mathrm{tp}} \tag{4}$$

where d_{hm} represents the tip-sample separation when the tip is at its home position, d_0 stands for changes in the tip-sample gap due to the sample distortion or drift, h is the surface features height and represents the actual surface topography, and d_{tp} is the tip displacement due to the control command.

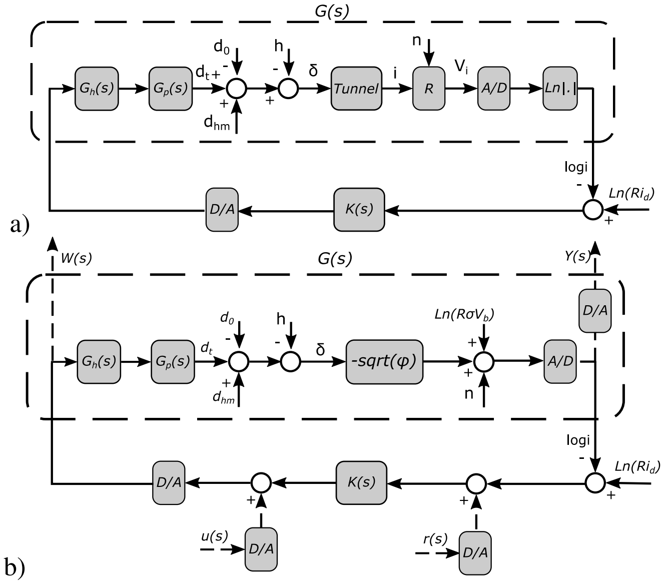

Fig. 2. (a) Block diagram of the STM z-axis control System. (b) Control block diagram with simplified tunneling current model. Exogenous inputs and outputs for identification purposes are shown in dashed arrows, and $s = j\omega$ is used.

Fig. 2(a) displays a block diagram of the closed-loop current control system of the STM. δ is converted to a current i through the tunneling current physics. The preamplifier converts this sub-nanoampere range current into a measurable voltage V_i which is then sampled by an A/D converter. Natural logarithm of the measured signal is first taken, then it is compared to the logarithm of the setpoint current $\ln(\mathrm{Ri}_d)$ to determine the error signal based on which a controller $K(s)$ operates. The control command passes through the D/A converter and the high-voltage amplifier $G_h(s)$ moves the piezo-actuator $G_p(s)$ and modifies δ. While scanning, the surface topography appears as an unknown disturbance h and results in a change in the tunneling current. The controller adjusts the vertical position of the tip to keep the current constant. Thus, the control command maps the surface topography. Misalignment of the sample or drift generates another disturbance d_0 while noise n is mainly generated with current measurement. The STM open-loop z-axis model is shown by $G(s)$ in Fig. 2(a) which represents all the dynamics from control command to $\log(i)$ signal.

Assuming a model given by (1) for the tunneling current and using (2), the closed-loop control block diagram is simplified, as shown in Fig. 2(b). Thus, the square root of φ appears as a gain. In the rest of this paper, we use the simplified block diagram shown in Fig. 2(b) for our discussion.

III. Stability and Performance Analysis

A. Closed-Loop System Identification

Fig. 2(b) depicts the experimental setup to identify the dynamics of STM closed-loop system. Frequency response functions (FRFs) were obtained for TFs from inputs u and r to outputs W and Y. Measurements were repeated 50 times and averaged to reduce the effect of sensor noise, the four underlying systems are

TABLE I
Identified Model Parameters

m	1	2	3
$p_m(kHz)$	8.25	9.11	12.2
$\eta_m \times 1000$	5.0	3.5	25
$f_m(kHz)$	8.65	9.69	–
$\zeta_m \times 1000$	8.5	15	–

$$G^c_{r2w}(j\omega) = \frac{W(j\omega)}{r(j\omega)} = \frac{z(j\omega)K(j\omega)z(j\omega)}{1 + K(j\omega)z(j\omega)G(j\omega)} \tag{5}$$

$$G^c_{r2y}(j\omega) = \frac{Y(j\omega)}{r(j\omega)} = \frac{z(j\omega)K(j\omega)z(j\omega)G(j\omega)z(j\omega)}{1 + K(j\omega)z(j\omega)G(j\omega)} \tag{6}$$

$$G^c_{u2w}(j\omega) = \frac{W(j\omega)}{u(j\omega)} = \frac{z(j\omega)z(j\omega)}{1 + K(j\omega)z(j\omega)G(j\omega)} \tag{7}$$

$$G^c_{u2y}(j\omega) = \frac{Y(j\omega)}{r(j\omega)} = \frac{z(j\omega)z(j\omega)G(j\omega)z(j\omega)}{1 + K(j\omega)z(j\omega)G(j\omega)} \tag{8}$$

where $z(j\omega)$ describes the zero-order-hold model of the A/D and D/A blocks. To determine the open-loop model $G(j\omega)$, we can divide the closed-loop FRFs at each frequency point to obtain

$$G_1(j\omega) = \frac{G^c_{u2y}(j\omega)}{G^c_{u2w}(j\omega)} = z(j\omega)G(j\omega) \tag{9}$$

$$G_2(j\omega) = \frac{G^c_{r2y}(j\omega)}{G^c_{r2w}(j\omega)} = z(j\omega)G(j\omega). \tag{10}$$

Having a fixed sampling frequency, $z(j\omega)$ is known, and thus both $G_1(j\omega)$ and $G_2(j\omega)$ represent the same open-loop dynamics $G(j\omega)$ after a further division by $z(j\omega)$. We can also obtain the controller dynamics $K(j\omega)$ by dividing (5) by (7) and (6) by (8). This can be used for validation purposes since the dynamics of the controller are already known. It is worth noting that: 1) to avoid the appearance of nonlinearities in $\log(i)$; 2) to prevent tip-sample crash due to large oscillations near resonance frequencies; and 3) to maintain good signal-to-noise ratio (SNR) during the tests, the frequency range of interest is divided into several intervals over which the amplitude of the input signal is adjusted properly. For more discussion on the procedure and associated results see [20].

Once the open-loop FRF is obtained, a TF model is fit to the measured data. Fig. 3 shows an experimentally obtained FRF and the model fit to it. Only dominant resonances are considered while fitting the model which is obtained as

$$G(s) = CG_0(s) = \frac{Ce^{-Ts}\left(\frac{1}{2\pi f_0}s + 1\right)}{\frac{1}{2\pi p_0}s + 1} \times \prod_{m=1}^{N} \frac{\left(\frac{s}{2\pi f_m}\right)^2 + 2\zeta_m\left(\frac{s}{2\pi f_m}\right) + 1}{\left(\frac{s}{2\pi p_m}\right)^2 + 2\eta_m\left(\frac{s}{2\pi p_m}\right) + 1} \tag{11}$$

with $C = 56.9$ dB, $T = 70\ \mu$s, $p_0 = 1.1$ kHz, $f_0 = 11$ kHz, $s = j\omega$, and other parameters given as Table I.

This article has been accepted for inclusion in a future issue of this journal. Content is final as presented, with the exception of pagination.

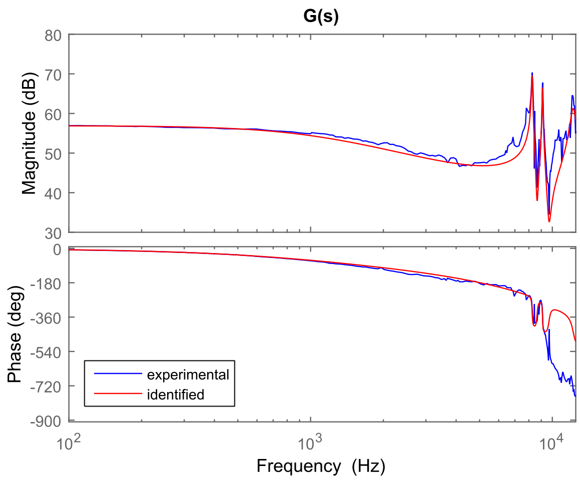

Fig. 3. FRF of the open-loop model $G(s)$ and the identified TF model.

B. Model Uncertainties

Some of the parameters in (11) change each time the STM is operated. After each tip replacement and due to the mechanical displacement of the tip holder in the scanner, the resonance frequencies are expected to change. Repeating identification tests showed that uncertainty in resonance frequencies is no more than 10% of their nominal value. Moreover, after the current is established the resonance frequencies are kept fixed since there is no significant mechanical motion in the tip holder.

Comparing FRF models of $G(s)$ obtained from successive measurements, we observed that the dc gain of the open-loop model $G(s)$ represented by parameter C in (11) is also subject to change. The observed range is 48–60 dB for the existing STM and a hydrogen passivated silicon wafer. Referring to the simplified block diagram shown in Fig. 2(b), we note that the dc gain of $G(s)$ is

$$C = -1.025\sqrt{\varphi}(a)_{H}\gamma \tag{12}$$

where A_H is the dc gain of high-voltage amplifier $G_h(s)$ and is constant ($A_H = 13.5$ in our setup). Also, γ is the dc gain of the piezo-actuator model $G_p(s)$ and depends on the piezo-actuator material and configuration. Since γ is constant as well, we may attribute observed variations in parameter C to the changes in parameter φ, i.e., the LBH. Regardless of the physical origin of LBH variations, one can find out from (12) that φ directly affects the closed-loop gain.

C. Closed-Loop Stability and Performance

We use the open-loop TF model given by (11) along with a PI controller to analyze the closed-loop stability and performance of the existing STM. The PI controller is given by

$$K(s) = k_i\left(\frac{1}{s} + \frac{1}{\omega_c}\right) \tag{13}$$

where k_i and ω_c represent the integrator gain (in s^{-1}) and the corner frequency of the controller (in rad/s), respectively. We first define the closed-loop stability and performance criteria, as follows.

1) Stability: Consider the loop TF with a unit integrator gain

$$G_{\mathrm{lp}}(s) = \left(\frac{1}{s} + \frac{1}{\omega_c}\right)G(s). \tag{14}$$

For a given ω_c, an integrator gain equal to the gain margin of the TF (14) makes the closed-loop system marginally stable. That is, we need $k_i < \mathrm{GM}\{G_{\mathrm{lp}}(s)\}$ for stability.

2) Bandwidth: The closed-loop bandwidth is typically required to be 100 times larger than that of the rastering frequency. The closed-loop imaging TF of the STM defined as

$$G_{\mathrm{img}}(s) = \frac{CK(s)}{1 + K(s)G(s)} \tag{15}$$

determines the closed-loop bandwidth.

3) Suppressed Ringing: To prevent the closed-loop system from exciting the piezo-actuator resonances, infinity norm of the imaging TF, must remain below a predefined threshold

$$\|G_{\mathrm{img}}(s)\|_\infty = \max_{\omega\in\mathbb{R}}\{|G_{\mathrm{img}}(j\omega)|\}. \tag{16}$$

These criteria define three curves in the PI controller parameter space. Selecting a value for ω_c, the critical integrator gain for marginal stability is given by (14). Repeating the procedure for various values of ω_c a curve shown by the solid line in Fig. 4(a) is obtained, to the left of which the stability criterion is satisfied. Also, selecting a desired minimum bandwidth ω_{BW} and following the same procedure using (15) leads to the dotted curve shown in Fig. 4(a) to the right of which the bandwidth criterion is satisfied. Selecting a desired maximum infinity norm and solving the nonlinear closed-loop equation for k_i, one obtains the dashed curve in Fig. 4(a) to the left of which criterion Section III-C3 is satisfied. Considering all three criteria, Fig. 4(a) suggests that PI gains must be selected in the colored area to ensure stability, fast and safe performance of the closed-loop system. Conventionally, half of the integrator gain that results in ringing is selected as the operating gain. This is shown by the black dashed-dotted curve in Fig. 4(a).

We have made experimental observations indicating that parameter C in (11) takes different values spanning approximately 10 dB in range. Such a large variation in C can easily affect stability and performance of the STM for which PI gains are already tuned. For instance, Fig. 4(b) shows stability and performance curves for the same system as shown in Fig. 4(a) but with parameter C being 6 dB larger. The appropriate PI gains area significantly shrinks when the dc gain soars to $C = 59.1$ dB, and if PI gains are tuned for a system with $C = 53.1$ dB the closed-loop system could experience ringing or become unstable. This observation suggests that once the PI gains are tuned and fixed, the LBH variations may deteriorate system performance. We believe this is a key cause of tip-sample crash in STM.

IV. Online LBH Estimation and PI Tuning

As shown in Fig. 2(b), we inject a dither signal with fixed frequency represented by $r(s)$ into the closed-loop system and track amplitude of the corresponding component in the

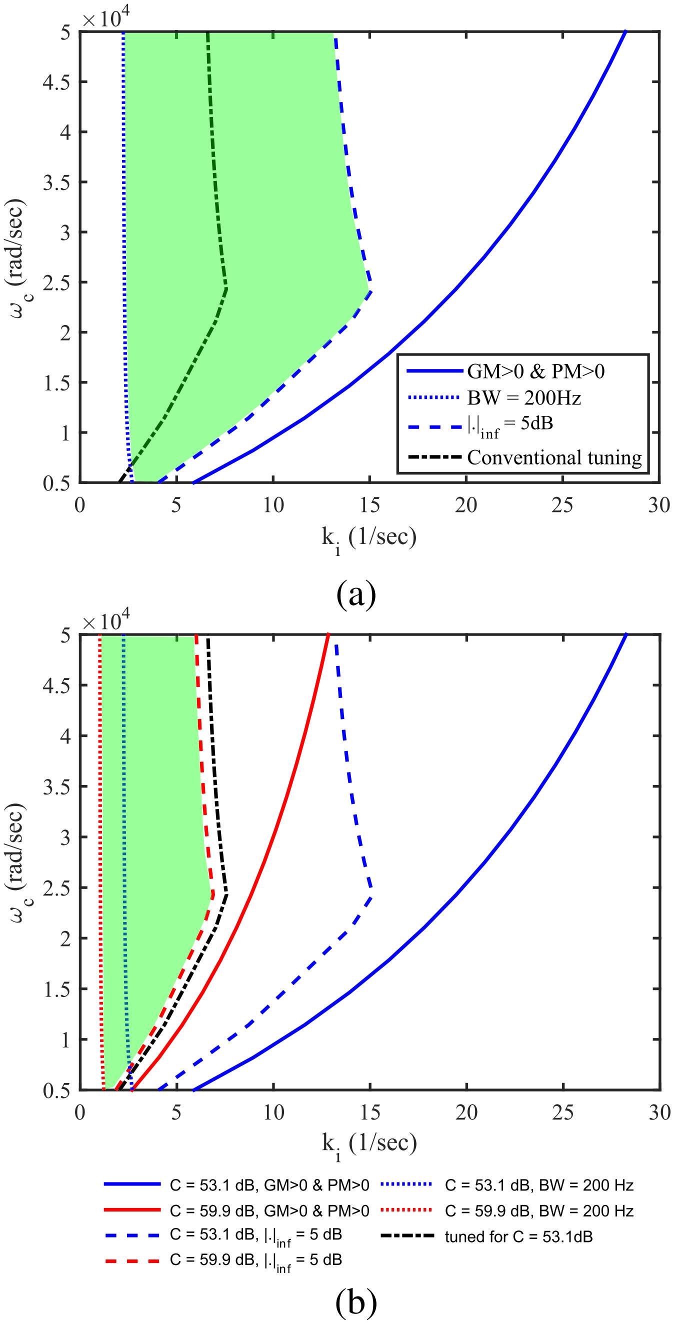

Fig. 4. (a) Critical stability and performance curves in the PI controller parameter space for a plant with $C = 53.1$ dB. Conventional tuning curve is shown as the black dashed-dotted curve, and colored area displays appropriate PI gains. (b) Shrinkage of the appropriate PI gains area for higher plant dc gain values. The tuned PI gains curve in (a) is outside of the colored appropriate area for the higher dc gain value in (b).

outputs Y and W. Lock-in amplifier is most commonly used for this purpose [33]. Here, we use an alternative amplitude estimation method based on Lyapunov filters [33]–[35].

A. LBH Estimation

The frequency Ω of the identification signal $r(j\Omega)$ should be greater than the closed-loop bandwidth so that it does not adversely affect the topography information at low frequencies. In addition, Ω should be small enough to avoid exciting resonance frequencies of the scanner. For the existing STM which requires a closed-loop bandwidth of a few hundred hertz and has its smallest resonance frequency near 8 kHz, we selected $\Omega = 4$ kHz.

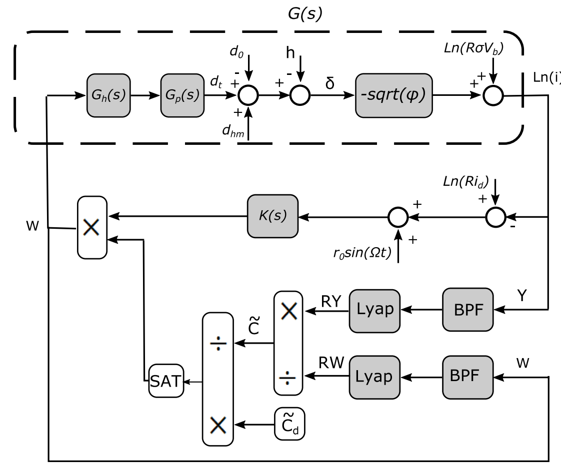

Fig. 5. z-axis control system block diagram with a self-tuning PI controller. The blocks shown by BPFs are through which the measured signals are passed prior to being fed into the Lyapunov filters. RY and RW are the amplitude of the Ω-component in the logarithm of tunneling current (Y) and the controller command (W), respectively. $\widetilde{C}$ is given by (20) and is proportional to the LBH. The block SAT is a saturation block which limits the modifying factor for safety reasons.

For LBH estimation, we are interested only in the Ω-component of Y and W. Thus, we pass the measured signals through a bandpass filter (BPF) centered at Ω before sending them to the Lyapunov filter. The passband of this filter determines the bandwidth of the LBH estimator. We assign a fixed 3-dB passband of 300 Hz around the center frequency of 4 kHz, and keep the adaptive gain of the Lyapunov filter as the only tunable parameter.

Schematics of the LBH estimation method are shown in Fig. 5. For a given $r(j\Omega)$, we may write

$$Y(j\Omega) = \frac{K(j\Omega)G(j\Omega)}{1+K(j\Omega)G(j\Omega)} r(j\Omega) \tag{17}$$

$$W(j\Omega) = \frac{K(j\Omega)}{1+K(j\Omega)G(j\Omega)} r(j\Omega). \tag{18}$$

Dividing (17) by (18) gives

$$\frac{Y(j\Omega)}{W(j\Omega)} = G(j\Omega) = \mathrm{C}G_0(j\Omega) \tag{19}$$

which may be rewritten in the real form as

$$\frac{\|Y(j\Omega)\|}{\|W(j\Omega)\|} = \frac{\mathrm{RY}}{\mathrm{RW}} = C\|G_0(j\Omega)\| = \widetilde{C}. \tag{20}$$

Since the resonances of the open-loop plant do not change after the tip and sample are engaged, i.e., $\|G_0(j\Omega)\|$ is constant, any variation in $\widetilde{C}$ of (20) relates to the changes in parameter C and originates from the LBH variations. Note that $\widetilde{C}$ is proportional to the absolute value of the plant dc gain C. Thus, whenever actual LBH is lower the obtained $\widetilde{C}$ is higher. This is due to the negative sign in (2).

It can be shown that the port at which the exogenous signal is added does not affect (20). However, since W is a small signal, we found that adding $r(j\Omega)$ to the setpoint leads to a better SNR at frequency Ω at both measured outputs. To this end, we point out that an alternative method for LBH estimation was proposed in the earlier STM literature. The differences

This article has been accepted for inclusion in a future issue of this journal. Content is final as presented, with the exception of pagination.

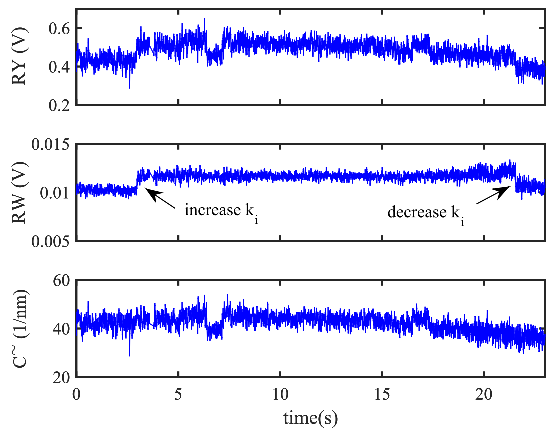

Fig. 6. RY, RW, and $\widetilde{C}$ as described in Fig. 5. The controller gain k_i is increased from 2.5 to 3.5 s^{-1} and is lowered back to its initial value. It is observed that these changes do not affect $\widetilde{C}$ as expected by (20).

between the two methods and, in particular, the advantages of the method proposed here are detailed in [17].

B. PI Tuning Based on LBH Estimation

It is possible to compensate for LBH variations by adapting the controller gain as

$$(k_i)_{\text{new}} = k_i \frac{\widetilde{C}_d}{\widetilde{C}}. \tag{21}$$

Here, $\widetilde{C}$ is the estimated dc gain of the open-loop system, which is proportional to LBH, and $\widetilde{C}_d$ is the desired value for $\widetilde{C}$. Both integral and proportional gains are multiplied by the factor $\widetilde{C}_d/\widetilde{C}$. The desired parameter $\widetilde{C}_d$ is a user-defined parameter recommended to be selected in the mid-range of observed $\widetilde{C}$ variations. Also, we use a saturation block for safety reasons, as shown in Fig. 5.

V. Experimental Results

In this section, first we present the experimental results confirming that the LBH is a variable that depends on local effects. We then go on to present experimental results showing the effect of the self-tuning PI controller on the STM performance and the tip life cycle.

A. LBH Measurements

Fig. 6 displays the estimated parameter $\widetilde{C}$ along with RY and RW signals, as shown in Fig. 5, measured while the STM was idle with all user defined parameters fixed. At time $t \simeq 3$ s controller gain k_i was increased and subsequently decreased back to its initial value at $t \simeq 22$ s. Fig. 6 suggests that $\widetilde{C}$ is not affected by the controller gains and this agrees with (20).

Fig. 7 shows a plot of $\widetilde{C}$ measurements while the STM tip was changing frequently. In this case, the STM tip has two stable states. All control system parameters were fixed during data collection. The STM was engaged, but not scanning. Tip changes are believed to be a major cause of the sudden changes in the LBH.

Fig. 8 further establishes the fact that LBH effects are highly localized. While the STM was idle, first the tip was moved laterally from point A to point B several nanometers away.

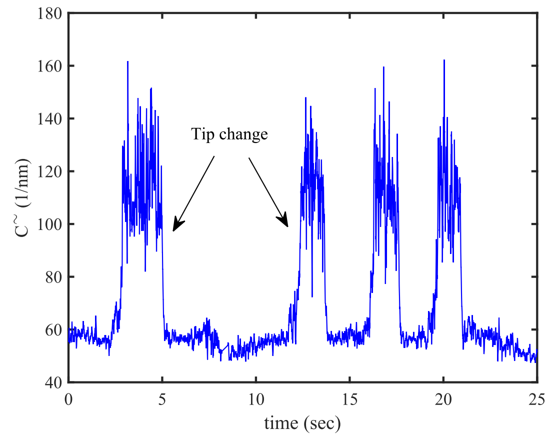

Fig. 7. $\widetilde{C}$ measured while the STM is engaged but otherwise idle. Tip changes causes sharp variations in the LBH.

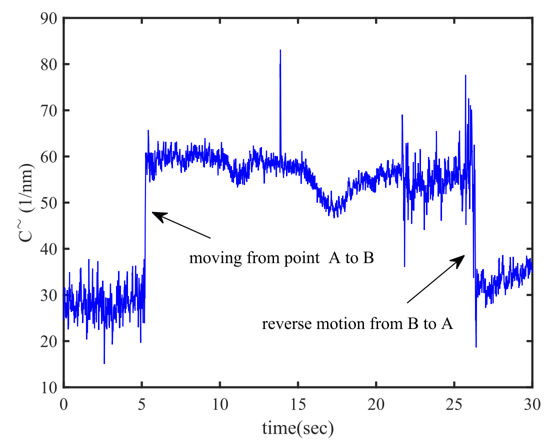

Fig. 8. $\widetilde{C}$ measured while the tip is moved from some point A to point B and is then returned to point A again. All other parameters are fixed.

It was then it was moved back to point A. Substantial changes observed in $\widetilde{C}$ suggest that the electronic/chemical properties of the atoms tunneled through at point A are different from those of atoms at point B resulting in different LBH values at the two points. This observation confirms that, while scanning, the LBH can undergo significant variations depending on the chemical composition of the sample surface.

The presented observations confirm that the plant dc gain can take significantly different values, while STM is operating. These variations originate from the tip changes, atomic structure of the sample or any other possible physical source. In addition, these observations suggest the need for continuous tuning of controller gains to prevent instabilities due to dc gain variations.

B. Self-Tuning PI Controller

We conducted several experiments to investigate the stabilizing effect of the PI tuning algorithm proposed in Section IV-B. LBH is measured at $\Omega = 1$ kHz with the Lyapunov filter gain set to $\zeta = 1000$. In order to show the stabilizing effect of the tuning algorithm, PI gains are intentionally set to a

This article has been accepted for inclusion in a future issue of this journal. Content is final as presented, with the exception of pagination.

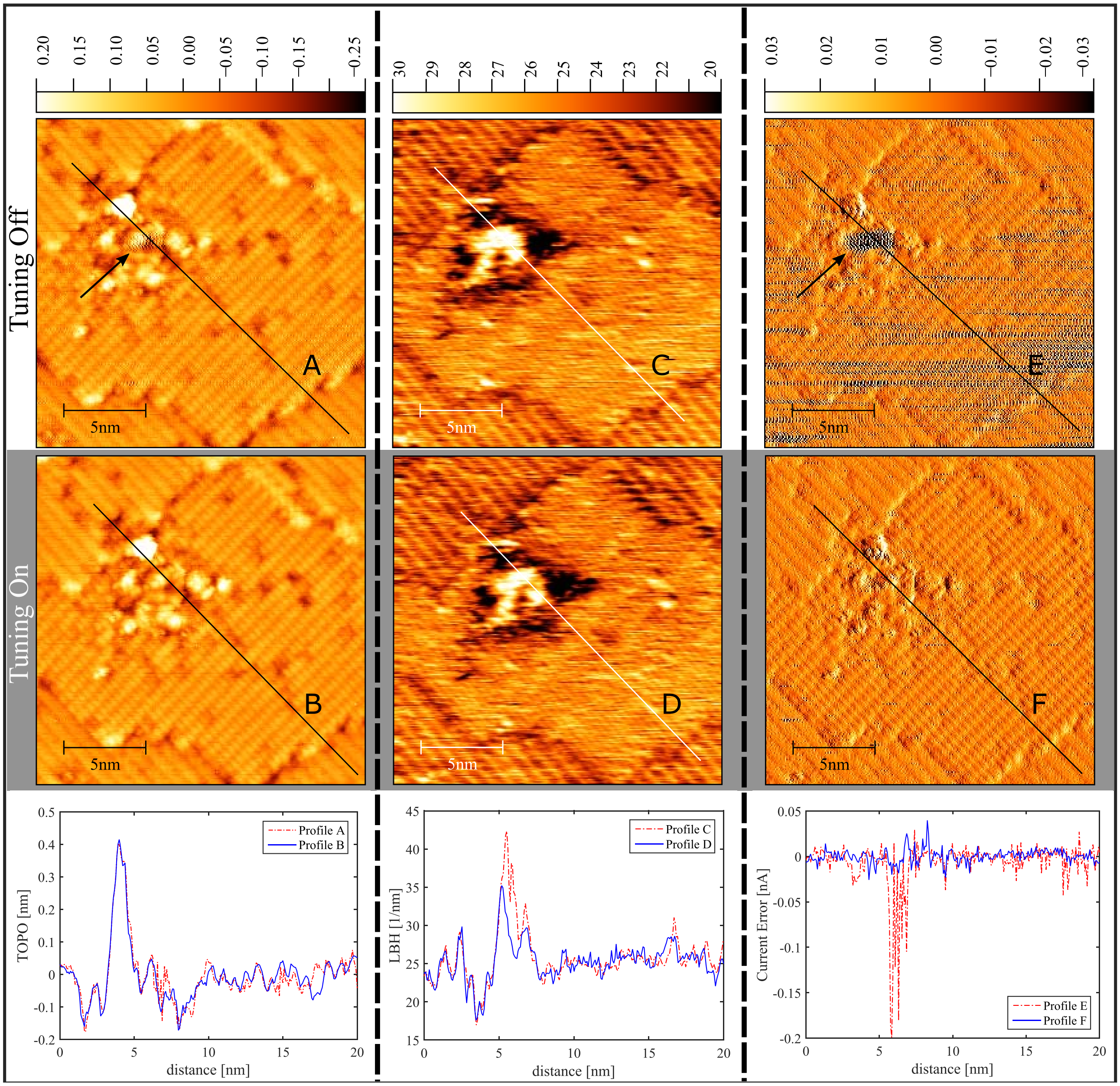

Fig. 9. PI tuning effects on the STM performance. Topography (left column), $\widetilde{C}$ representing the LBH (middle column), and current error (right column) images for the two cases without PI tuning (top row) and with PI tuning (middle row). Plots at the bottom row show the profiles drawn on the corresponding images above. PI gains are high and the system is close to the stability margin. Surface atomic and electronic structures are visibly different close to the center of the sample due to contamination or previous tip contact. While passing over the low-LBH (high $\widetilde{C}$) area, the closed-loop system experiences ringing when the PI tuning is inactive. Immediately after the first test, PI tuning is activated and the surface is rescanned. The closed-loop system does not experience ringing with active PI tuning. Ringing appears as artifact in topography image, e.g., area near profiles A and E pointed to by arrows.

high value to bring the feedback loop close to the stability margin. Due to contamination or previous tip-sample contact, an area of low LBH (high $\widetilde{C}$) value exists on the hydrogen passivated silicon surface shown in Fig. 9. First, we deactivated the tuning algorithm and scanned the surface with fixed gain. When passing over the low-LBH area, the feedback system undergoes ringing. The instability is apparent in current error image (profile F in Fig. 9). Note that this happens only over the atoms with low LBH, while over the neighboring atoms with large topography and normal LBH, the feedback system is still stable.

Immediately after the first test, we activated the tuning algorithm and rescanned the surface while all other parameters including the initial PI gains were preserved. As shown in the middle row of Fig. 9, the feedback loop remains stable despite large variations in the LBH. Comparison of profiles F and E in Fig. 9 shows that with the PI tuning algorithm the current is better kept constant. Profile D in Fig. 9 shows that $\widetilde{C}$ in the contaminated area is approximately 50% larger than other locations on the surface. This explains the feedback instability in that area with fixed PI gains. While the PI tuning is inactive and the feedback system is ringing, LBH estimation

This article has been accepted for inclusion in a future issue of this journal. Content is final as presented, with the exception of pagination.

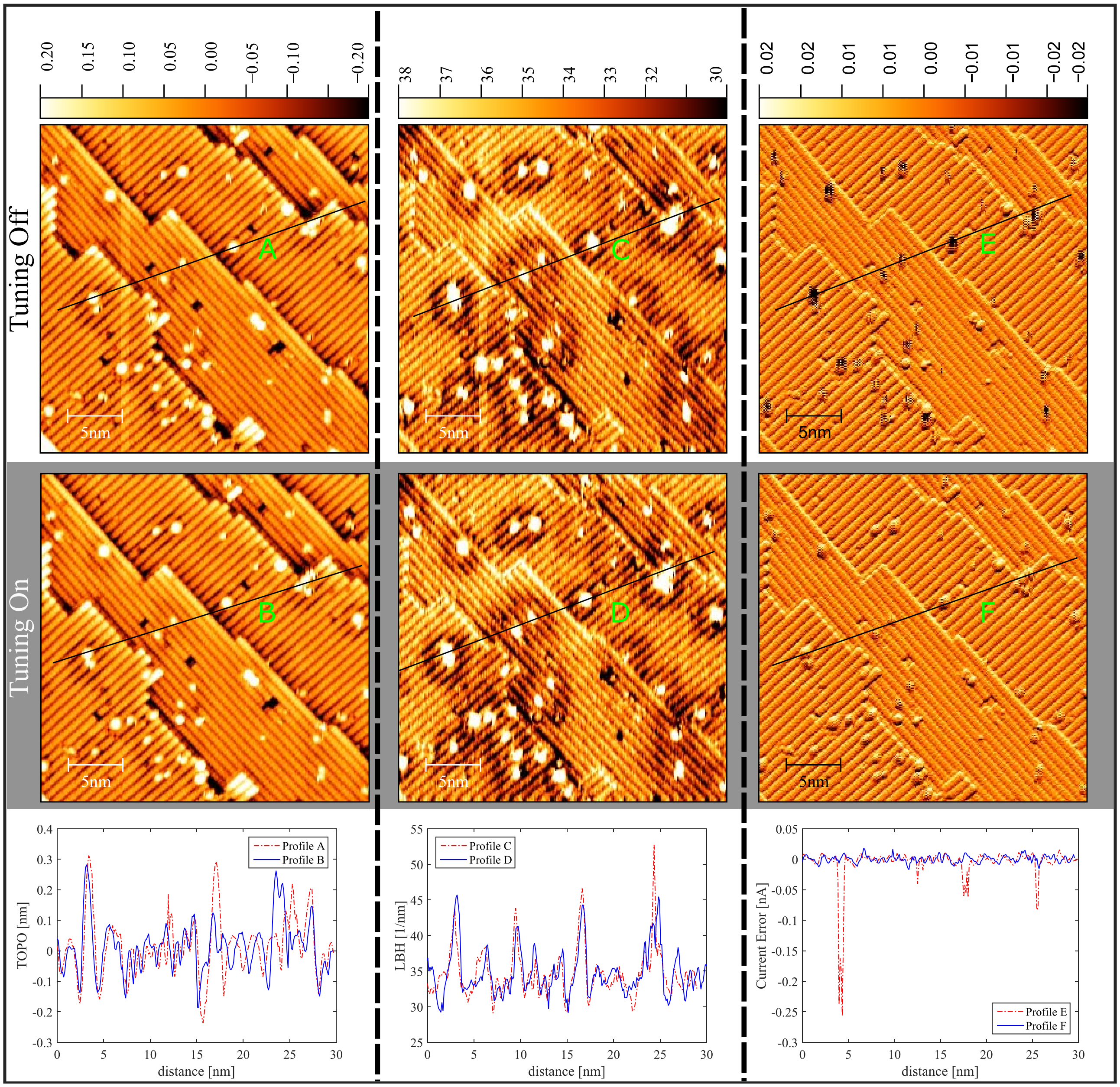

Fig. 10. PI tuning effect on the STM performance. The surface is clean with several dangling bonds which represent missing hydrogen atoms. PI gains are high and the surface is scanned successively with PI tuning OFF (top row) and ON (middle row). All other parameters are the same in the two tests. Over the dangling bonds, the estimated $\widetilde{C}$ is larger, and this causes ringing when the PI tuning is OFF as evidenced by profile E. When the tuning is active, the feedback system remains stable and no artifact is observed.

results shown in Fig. 9 are not reliable. A comparison of the topography images and profiles A with B in Fig. 9 confirms that feedback instability causes artifacts in the acquired STM image, while with the PI tuning these artifacts are removed.

We repeated the same experiment on a different sample and with a different tip. Obtained results are shown in Fig. 10. In this experiment, we had a clean hydrogen passivated silicon surface with several dangling bonds representing missing hydrogen atoms that appear as bright dots in the topography images. Over the dangling bonds the LBH is lower and the measured $\widetilde{C}$ is higher as shown by profiles C and D in Fig. 10. We used a set of PI gains that put the system close to the stability margin when PI tuning is inactive. While passing over the dangling bonds, the feedback system experiences ringing as shown by profile E in Fig. 10. After the PI tuning is activated, the system operates reliably and produces clean images without artifacts while the initial PI gains are still high.

C. Tip Life Cycle

To perform the experiments reported in Section V-B, we brought the system close to the stability margin by using high PI gains. Although such high gains are not normally

This article has been accepted for inclusion in a future issue of this journal. Content is final as presented, with the exception of pagination.

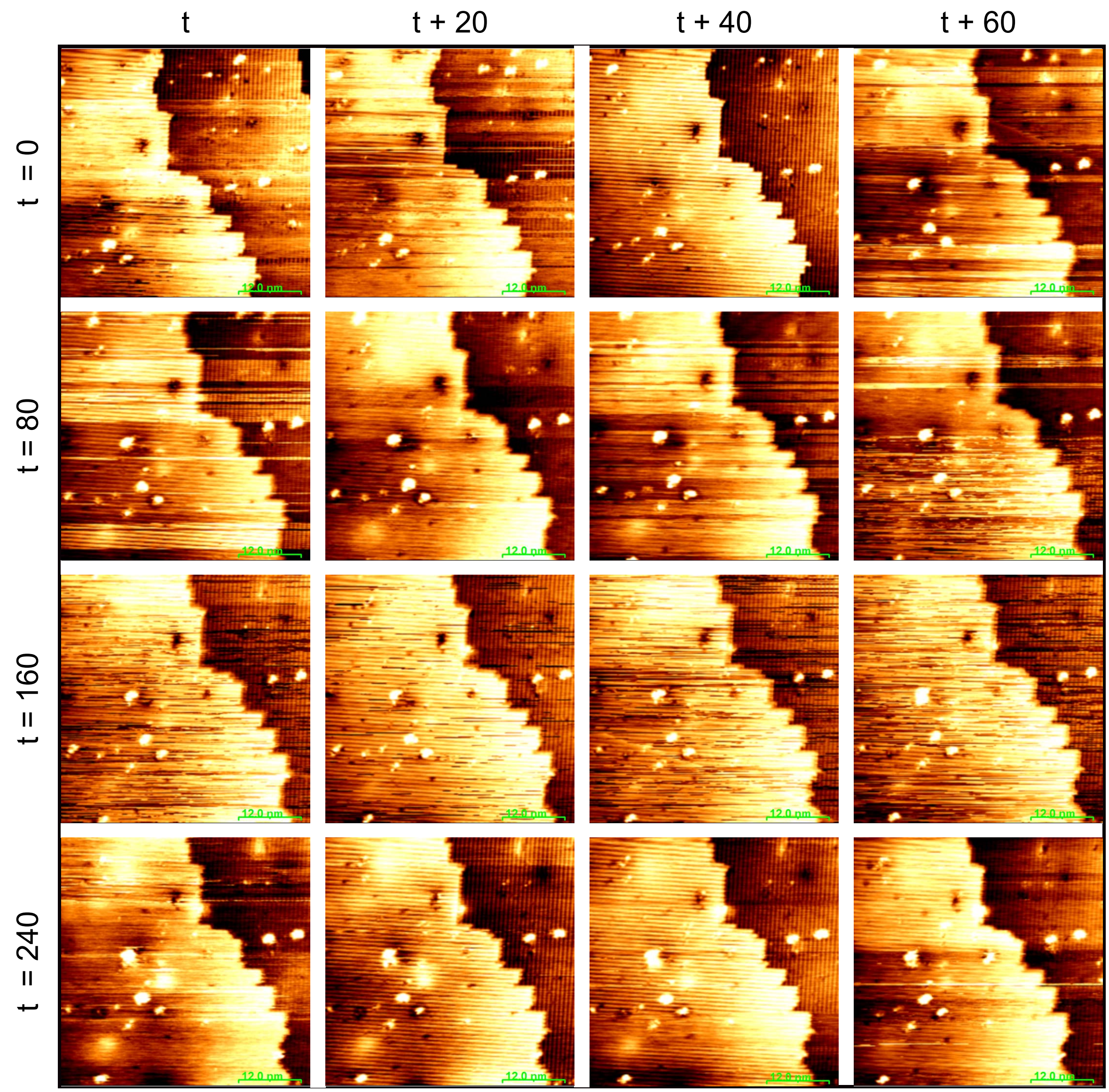

Fig. 11. Successive scanning of hydrogen passivated Si surface with self-tuning PI controller. Frame times are given in minutes relative to the image in the top left corner. PI gains are normal and scanning speed is 150 nm/s. One out of four captured images are shown. Horizontal color changes indicate tip changes. The closed-loop stays stable and no visible change to the surface arises from imaging.

used in STM operation, they support the claim that the LBH may lead to closed-loop instability. Moreover, high PI gains help to capture the LBH stability effects in a single experiment. Under normal working conditions, LBH stability effects may appear gradually and influence the tip life cycle.

We successively scanned a hydrogen passivated Si surface, while the PI gains and scanning speed were normal, and the tuning algorithm was operating. After collecting 64 images each taking 5 min, we switched OFF the tuning algorithm and continued the successive scanning with the same parameters. Figs. 11 and 12 show one out of four captured images with the PI tuning algorithm and without it, respectively. Fig. 11 shows that, while the tuning algorithm was active, the tip changes did not result in a major crash. However, with the tuning being inactive in Fig. 12, tip changes resulted in formation of undesired patterns on the surface as visible in Fig. 12. These patterns are formed due to some unknown tip-sample interaction that results in the removal of hydrogen atoms from the surface. LBH properties of these regions are similar to dangling bonds. The growth of the formed pattern in the next scans and the final tip crash can be due to the variation of the LBH caused by the tip changes and by the formed patterns.

Fig. 12 images suggest that closed-loop instabilities may originate from tip changes and in turn damage both the tip and the surface. Tip changes are visible in both Figs. 11 and 12 as horizontal sharp color changes. With PI gains fixed in Fig. 12, LBH variations originated from sudden tip changes cause closed-loop ringing and initiate formation of undesired patterns on the surface. LBH is different over the patterned spots which makes the situation worse in successive scans.

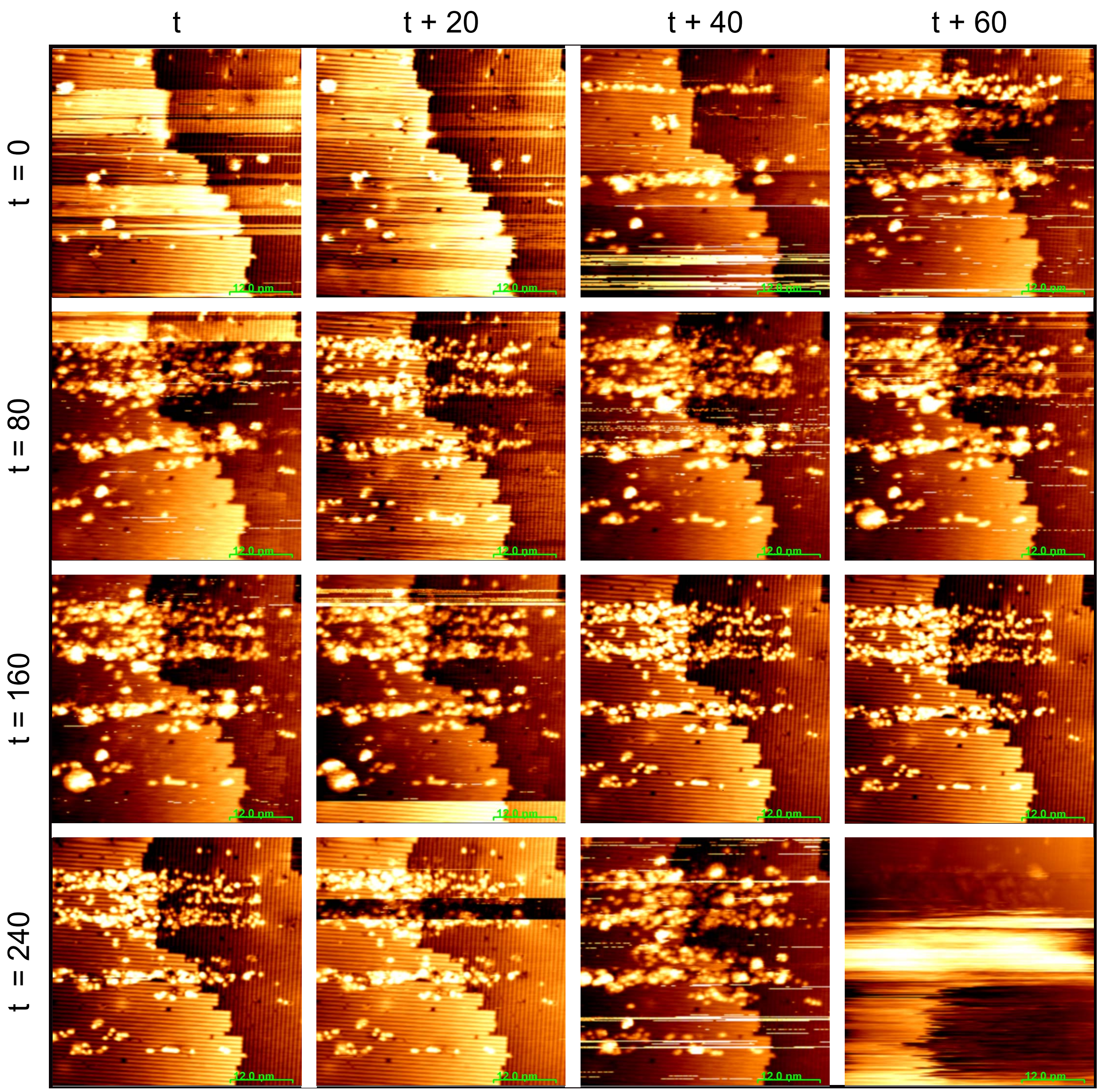

Fig. 12. Successive scanning of the same sample as in Fig. 11 with the same tip and parameters, while the self-tuning PI controller is inactive. Tip changes occur in the first images, then hydrogen depassivation patterns form on the surface close to the spots that the tip changes had occurred. Formation of such patterns and their growth in the following images are believed to be due to the unsafe decrease in the tip sample separation caused by the closed-loop instability. LBH variations arising from the tip changes and the depassivated patterns can be the reason for instability. The tip crashes into the surface at the end.

VI. Conclusion

We analyzed the control system of an STM. Frequency-domain closed-loop system identification tests were conducted to obtain open-loop models of the STM. Our analysis shows that dc gain of the open-loop plant is proportional to the LBH which is a quantum mechanical property of the tip and the sample. The LBH is known to be a variable parameter in STM which depends on many local effects. We showed that the LBH variation can dramatically change the loop gain in the presence of a controller with fixed parameters and this can easily result in closed-loop instability. We proposed an algorithm for online LBH estimation and used the obtained estimation to adaptively tune the PI controller gains. The estimated LBH is also used for generating LBH images which map electronic properties of the surface.

Experimental results confirm that the LBH is a varying parameter, and that the proposed method is effective in enhancing the closed-loop stability. Furthermore, the proposed tuning method allows for safe increase of PI gains that in turn results in higher closed-loop bandwidth and enables high-speed scanning. Further experimental results confirm the effect of the proposed control method on protecting the tip and extending its life cycle by lowering the chance of the tip/sample crash.

Acknowledgment

The authors would like to thank J. Ballard, E. Fuchs, and J. Owen from Zyvex Labs and S. Schmucker from NIST for fruitful discussions, and Zyvex Labs' technicians C. Delgado and R. Santini for their help and collaboration.

References

[1] R. A. Wolkow, "Direct observation of an increase in buckled dimers on Si(001) at low temperature," *Phys. Rev. Lett.*, vol. 68, no. 17, pp. 2636–2639, 1992.

[2] T. Zhang *et al.*, "Experimental demonstration of topological surface states protected by time-reversal symmetry," *Phys. Rev. Lett.*, vol. 103, no. 26, pp. 1–4, 2009.

[3] P. K. Hansma, V. B. Elings, O. Marti, and C. E. Bracker, "Scanning tunneling microscopy and atomic force microscopy: Application to biology and technology," *Science*, vol. 242, pp. 209–216, Oct. 1988.

[4] S. Loth, M. Etzkorn, C. P. Lutz, D. M. Eigler, and A. J. Heinrich, "Measurement of fast electron spin relaxation times with atomic resolution," *Science*, vol. 329, no. 5999, pp. 1628–1630, 2010.

[5] J. W. Lyding, T. C. Shen, J. S. Hubacek, J. R. Tucker, and G. C. Abeln, "Nanoscale patterning and oxidation of H-passivated Si(100)-2×1 surfaces with an ultrahigh vacuum scanning tunneling microscope," *Appl. Phys. Lett.*, vol. 64, no. 15, pp. 2010–2012, 1994.

[6] J. B. Ballard *et al.*, "Multimode hydrogen depassivation lithography: A method for optimizing atomically precise write times," *J. Vac. Sci. Technol. B, Microelectron. Process. Phenom.*, vol. 31, no. 6, p. 06FC01, 2013.

[7] M. Fuechsle *et al.*, "A single-atom transistor," *Nature Nanotechnol.*, vol. 7, no. 4, pp. 242–246, 2012.

[8] B. Weber *et al.*, "Ohm's law survives to the atomic scale," *Science*, vol. 335, pp. 64–67, Jan. 2012.

[9] W. C. T. Lee *et al.*, "Lithography and doping in strained Si towards atomically precise device fabrication," *Nanotechnology*, vol. 25, no. 14, p. 145302, 2014.

[10] A. I. Oliva, E. Anguiano, N. Denisenko, M. Aguilar, and J. L. Peña, "Analysis of scanning tunneling microscopy feedback system," *Rev. Sci. Instrum.*, vol. 66, no. 5, p. 3196, 1995.

[11] E. Anguiano, A. I. Oliva, and M. Aguilar, "Optimal conditions for imaging in scanning tunneling microscopy: Theory," *Rev. Sci. Instrum.*, vol. 69, no. 11, p. 3867, 1998.

[12] A. I. Oliva, M. Aguilar, J. L. Peña, and E. Anguiano, "Experimental determination of the parameters of the feedback system of a scanning tunnelling microscope," *Meas. Sci. Technol.*, vol. 8, no. 5, pp. 501–507, 1997.

[13] I. Ahmad, A. Voda, and G. Besancon, "Controller design for a closed-loop scanning tunneling microscope," in *Proc. IEEE Int. Conf. Autom. Sci. Eng.*, Washington, DC, USA, vol. 2, Aug. 2008, pp. 971–976.

[14] I. Ahmad, A. Voda, G. Besançon, and G. Buche, "Robust digital control approach for high performance tunneling current measurement system," *Control Eng. Pract.*, vol. 20, no. 7, pp. 643–653, 2012.

[15] N. Bonnail, D. Tonneau, F. Jandard, G. A. Capolino, and H. Dallaporta, "Variable structure control of a piezoelectric actuator for a scanning tunneling microscope," *IEEE Trans. Ind. Electron.*, vol. 51, no. 2, pp. 354–363, Apr. 2004.

[16] S. Blanvillain, A. Voda, G. Besancon, and G. Buche, "Subnanometer positioning and drift compensation with tunneling current," *IEEE Trans. Control Syst. Technol.*, vol. 22, no. 1, pp. 180–189, Jan. 2014.

[17] F. Tajaddodianfar, S. O. R. Moheimani, J. Owen, and J. N. Randall, "On the effect of local barrier height in scanning tunneling microscopy: Measurement methods and control implications," *Rev. Sci. Instrum.*, vol. 89, no. 1, p. 013701, 2018.

[18] F. Tajaddodianfar, S. O. R. Moheimani, J. Owen, and J. N. Randall, "A self-tuning controller for high-performance scanning tunneling microscopy," in *Proc. IEEE Conf. Control Technol. Appl. (CCTA)*, Honolulu, HI, USA, Aug. 2017, pp. 106–110.

[19] F. Tajaddodianfar, S. O. R. Moheimani, E. Fuchs, and J. N. Randall, "Stability analysis of a scanning tunneling microscope control system," in *Proc. Amer. Control Conf. (ACC)*, Seattle, WA, USA, May 2017, pp. 204–209.

[20] F. Tajaddodianfar, A. Fowler, E. Fuchs, J. N. Randall, and S. O. R. Moheimani, "Frequency-domain closed-loop system identification of a scanning tunneling microscope," in *Proc. ASPE Spring Topical Meeting Precis. Mech. Syst. Design Control*. Cambridge, MA, USA: Massachusetts Institute of Technology, 2016, pp. 54–57.

[21] G. Binnig, N. Garcia, H. Rohrer, J. M. Soler, and F. Flores, "Electron-metal-surface interaction potential with vacuum tunneling: Observation of the image force," *Phys. Rev. B, Condens. Matter*, vol. 30, no. 8, pp. 4816–4818, 1984.

[22] G. Binnig and H. Rohrer, "Scanning tunneling microscopy," *IBM J. Res. Develop.*, vol. 44, nos. 1–2, pp. 279–293, 2000.

[23] Y. Maeda, M. Okumura, S. Tsubota, M. Kohyama, and M. Haruta, "Local barrier height of Au nanoparticles on a TiO_2(1 1 0)-(1×2) surface," *Appl. Surf. Sci.*, vol. 222, nos. 1–4, pp. 409–414, 2004.

[24] N. D. Lang, "Apparent barrier height in scanning tunneling microscopy," *Phys. Rev. B, Condens. Matter*, vol. 37, no. 17, p. 10395–10398, 1988.

[25] M. Saida, K. Horikawa, T. Sato, S. Yamamoto, and M. Sasaki, "Local tunneling barrier height observations of NiAl(1 1 0)," *Surf. Sci.*, vol. 600, no. 11, pp. L139–L142 2006.

[26] A. Sugimoto, T. Ekino, and H. Eisaki, "Nanoscale modulation of local barrier height on Bi-based cuprate superconductors observed by scanning tunneling microscopy/spectroscopy," *J. Phys. Soc. Jpn.*, vol. 77, no. 4, pp. 14–17, 2008.

[27] U. Forssell and L. Ljung, "Closed-loop identification revisited," *Automatica*, vol. 35, no. 7, pp. 1215–1241, 1999.

[28] N. Garcia, C. Ocal, and F. Flores, "Model theory for scanning tunneling microscopy: Application to Au(110) (1×2)," *Phys. Rev. Lett.*, vol. 50, no. 25, pp. 2002–2005, 1983.

[29] B. Voigtlander, *Scanning Probe Microscopy: Atomic Force Microscopy and Scanning Tunneling Microscopy*. Berlin, Germany: Springer-Verlag, 2015.

[30] Y. Kuk, "Scanning tunneling spectroscopy of metal surfaces," *J. Vac. Sci. Technol. A, Vac. Surf. Films*, vol. 8, no. 1, p. 289, 1990.

[31] R. Wiesendanger *et al.*, "Local tunneling barrier height images obtained with the scanning tunneling microscope," *Surf. Sci.*, vols. 189–190, pp. 24–28, Oct. 1987.

[32] J. F. Jia, K. Inoue, Y. Hasegawa, W. S. Yang, and T. Sakurai, "Variation of the local work function at steps on metal surfaces studied with STM," *Phys. Rev. B, Condens. Matter*, vol. 58, pp. 1193–1196, Jul. 1998.

[33] M. G. Ruppert, D. M. Harcombe, M. R. Ragazzon, S. O. R. Moheimani, and A. J. Fleming, "A review of demodulation techniques for amplitude-modulation atomic force microscopy," *Beilstein J. Nanotechnol.*, vol. 8, no. 1, pp. 1407–1426, 2017.

[34] M. R. Ragazzon, M. G. Ruppert, D. M. Harcombe, A. J. Fleming, and J. T. Gravdahl, "Lyapunov estimator for high-speed demodulation in dynamic mode atomic force microscopy," *IEEE Trans. Control Syst. Technol.*, vol. 26, no. 2, pp. 765–772, Mar. 2017.

[35] D. M. Harcombe, M. G. Ruppert, M. R. Ragazzon, and A. J. Fleming, "Higher-harmonic AFM imaging with a high-bandwidth multifrequency Lyapunov filter," in *Proc. IEEE/ASME Int. Conf. Adv. Intell. Mechatronics (AIM)*, Jul. 2017, pp. 725–730.

Farid Tajaddodianfar received the B.S. degree in mechanical engineering from the K. N. Toosi University of Technology, Tehran, Iran, in 2007, the M.S. degree in mechanical engineering from the Sharif University of Technology, Tehran, in 2010, and the Ph.D. degrees in mechanical engineering from the University of Tehran, Tehran, and the University of Texas at Dallas, Richardson, TX, USA, in 2015 and 2018, respectively.

He joined Microsoft, Redmond, WA, USA, as an Applied Researcher in 2018. He has authored over 25 publications including peer-reviewed journal papers, proceedings, and a U.S. patent with >180 citations. His current research interests include applied mathematics and statistics, nonlinear dynamics, estimation and control, artificial intelligence, and machine learning.

Dr. Tajaddodianfar was a recipient of the Louis J. Beecherl Fellowship in 2017 for his outstanding academic performance.

S. O. Reza Moheimani (F'11) is currently the James Von Ehr Distinguished Chair in science and technology with the Department of Mechanical Engineering, University of Texas at Dallas, Richardson, TX, USA. He is also an Adjunct Professor with the University of Newcastle, NSW, Australia. His current research interests include ultrahigh-precision mechatronic systems, with particular emphasis on dynamics and control at the nanometer scale, including applications of control and estimation in nanopositioning systems for high-speed scanning probe microscopy and nanomanufacturing, modeling and control of microcantilever-based devices, control of microactuators in microelectromechanical systems, and design, and modeling and control of micromachined nanopositioners for on-chip scanning probe microscopy and atomically precise lithography.

Dr. Moheimani is a fellow of the IFAC and the Institute of Physics, U.K. He was a recipient of the IFAC Nathaniel B. Nichols Medal in 2014, the IFAC Mechatronic Systems Award in 2013, the IEEE Control Systems Technology Award in 2009, the IEEE Transactions on Control Systems Technology Outstanding Paper Award in 2007, and several best paper awards in various conferences. He is the Editor-in-Chief of Mechatronics and has served on the editorial boards of a number of other journals, including the IEEE TRANSACTIONS ON MECHATRONICS, the IEEE TRANSACTIONS ON CONTROL SYSTEMS TECHNOLOGY, and *Control Engineering Practice*. He is the Chair of the IFAC Technical Committee on Mechatronic Systems 2011-2017.

John N. Randall (F'15) received the B.S., M.S., and Ph.D. degrees in electrical engineering from the University of Houston, Houston, TX, USA.

He is currently a President with Zyvex Labs, Richardson, TX, USA, an Executive VP at NanoRetina, Richardson, TX, USA, and an Adjunct Professor at UT Dallas, Richardson, TX, USA. He has over 30 years of experience in micro- and nano-fabrication. He joined Zyvex in 2001. He was with M.I.T. Lincoln Laboratory, Lexington, MA, USA, where he was involved in ion beam and x-ray lithography. He was with Texas Instruments, Dallas, TX, USA, where he was a Distinguished Member of the Technical Staff. He was with IMEC, Leuven, Belgium, where he was involved in high-resolution processing for integrated circuits, MEMS, quantum effect devices and advanced lithograph. He has authored over 109 articles in refereed journals, over 50 conference proceedings and other publications with >3800 citations, and 31 issued U.S. patents with >800 citations.

Dr. Randall is a fellow of the AVS. He received from UH a Distinguished Engineering Alumni Award.